ACS APPLIED MATERIALS & INTERFACES

Research Article

www.acsami.org

Tuning the Resonant Frequency of Resonators Using Molecular Surface Self-assembly Approach

Wenpeng Liu,[†] Jingwei Wang,[†] Yifei Yu,[†] Ye Chang,[†] Ning Tang,[†] Hemi Qu,[†] Yanyan Wang,[†] Wei Pang,[†] Hao Zhang,*[,†] Daihua Zhang,[†] Huaping Xu,[‡] and Xuexin Duan*[,†]

[†]State Key Laboratory of Precision Measuring Technology & Instruments, College of Precision Instrument and Optoelectronics Engineering, Tianjin University, Tianjin 300072, China

[‡]Key Lab of Organic Optoelectronics & Molecular Engineering, Department of Chemistry, Tsinghua University, Beijing 100084, China

Supporting Information

ABSTRACT: In this work, a new method to tune the resonant frequency of microfabricated resonator using molecular layer-by-layer (LbL) self-assembly approach is demonstrated. By simply controlling the polymer concentration and the number of layers deposited, precisely tuning the frequency of microfabricated resonators is realized. Due to its selective deposition through specific molecular recognitions, such technique avoids the high-cost and complex steps of conventional semiconductor fabrications and is able to tune individual diced device. Briefly, film bulk acoustic resonator (FBAR) is used to demonstrate the tuning process and two types of LbL deposition methods are compared. The film thickness and morphology have been characterized by UV−vis reflection spectra, ellipsometer and AFM. As a result, the maximum resonant frequency shift of FBAR reaches more than 20 MHz, meaning 1.4% tunability at least. The minimum frequency shift is nearly 10 kHZ per bilayer, indicating 7 ppm tuning resolution. Pressure cooker test (PCT) is performed to evaluate the reliability of LbL coated FBAR. Furthermore, applications for wireless broadband communication and chemical sensors of LbL coated FBAR have been demonstrated.

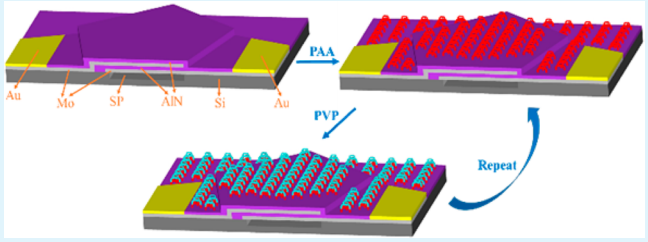

KEYWORDS: *resonators, layer-by-layer (LbL) self-assembly, film bulk acoustic resonator (FBAR), frequency tuning, gas sensor*

1. INTRODUCTION

The development of compact, low cost, high-performance resonators is meant to respond to the growing demand of single-chip, highly integrated sensor (arrays) for (bio)chemical sensing applications,[1−6] and multiband radio frequency (RF) solutions for advanced wireless communication systems.[7−10] Micro- and nanoelectromechanical (MEMS/NEMS) resonators for sensor and RF applications have been widely explored because of their small size, light weight, low loss, and high IC integration capability.[11−14] Recently, the development of nanomaterials such as nanotubes,[15,16] nanowires,[17] graphene,[18] and other 2D nanomaterials,[19] have opened new research interests in MEMS/NEMS resonator design and fabrications. In any case, micro/nano fabricated resonators are designed to work at appropriate frequency for specific applications. For instance, (bio)chemical resonator sensors are preferred to work at defined frequency where the frequency changes linearly to the analytes concentration and responses at large dynamic range. Besides, resonator sensor arrays need to work at the same resonant frequency to simplify the test system in applications such as real-time multiplexed sensing.[20] In the field of RF wireless communication, resonators are widely integrated into very large scale integrated circuits (VLSI) as filters, oscillators, phase locking loops (PLL) and other electronic components, all of them are supposed to operate at a given frequency in accordance with the peripheral circuit or communication protocol.[9,12,13] However, due to the variations in semiconductor fabrication processes, micro/nano fabricated resonators are prone to deviate from the desired working frequency and could have large resonant frequency distribution at wafer scale (see Supporting Information). The solution leads to the technique of "frequency tuning" which normally requires multisteps of semiconductor fabrications to adjust the thickness of the resonators. Other possible frequency tuning methods include control the actuation force driven by bias voltage or mechanical stress which result in changes in the resonance behaviors.[10,21,22] However, all these methods require professional operators and high-end equipment, and the process is time-consuming and cannot be applied to an individual diced device. Therefore, an accessible, friendly, and low-cost tuning method is highly desired.

In this work, we demonstrated a new method to tune the resonant frequency of microfabricated resonators via a molecular layer-by-layer (LbL) self-assembly approaches.

Received: November 2, 2014
Accepted: December 9, 2014
Published: December 9, 2014

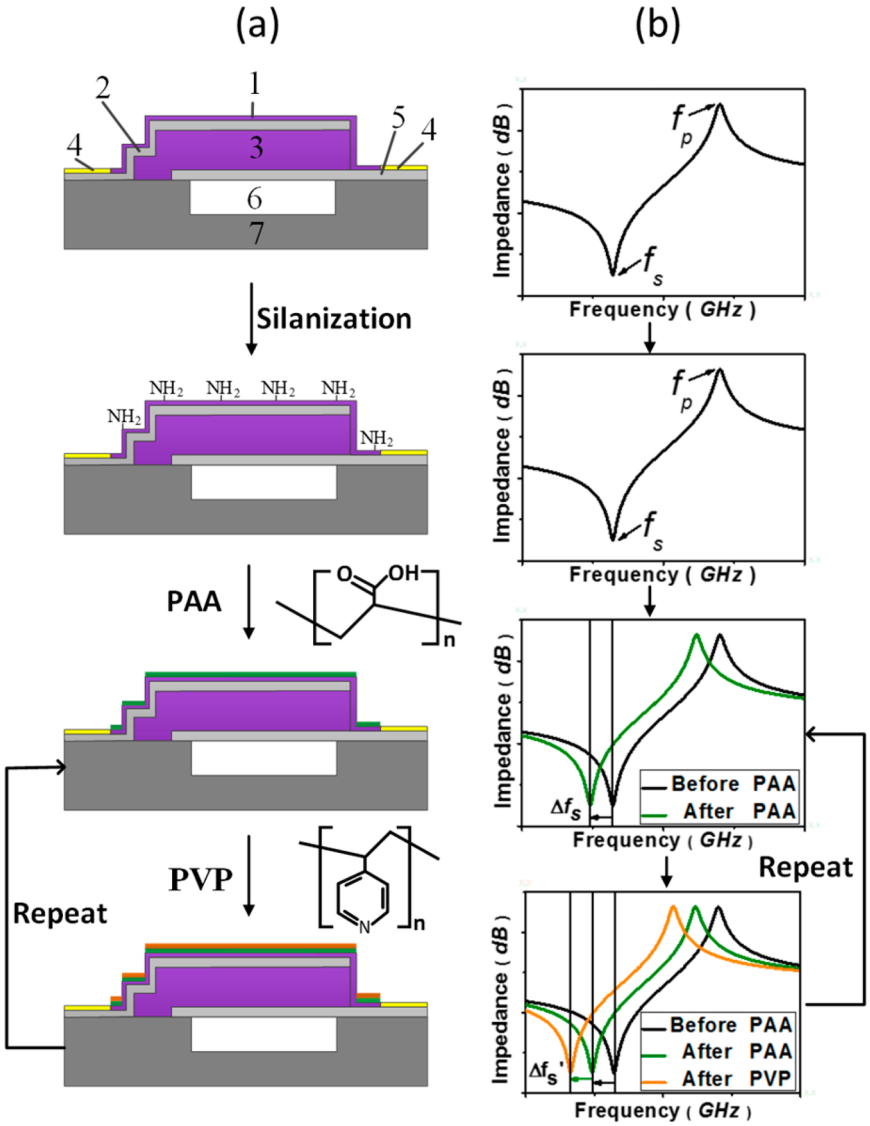

Figure 1. (a) Cartoon showing the growth of PAA/PVP bilayers on FBAR surface through molecular LbL self-assembly approach and (b) the series resonant frequency shift of FBAR according to the impedance characteristic. (1) PS layer, (2) TE, (3) PZ layer, (4) pad, (5) BE, (6) swimming pool (SP), and (7) silicon substrate.

Molecular LbL self-assembly is first introduced by assembling positively and negatively charged polyelectrolytes in a layer by layer fashion through electrostatic interactions.[23] It has been applied as an efficient surface modification technique for medical and biological applications.[24−26] Here, we utilize LbL assembly of poly(acrylic acid) (PAA) and poly(4-vinylpyridine) (PVP) on the resonator surface to tune the resonant frequency of a microfabricated thin film resonator—film bulk acoustic wave resonator (FBAR).[9] Due to its selective deposition onto the resonator surface without contaminating the gold pads with careful chemical design, the LbL tuning technique has the advantages of mask-less fabrication, high tuning resolution, and wide tuning range. It avoids the high-cost semiconductor process and is able to tune the individual device to the desired frequency. Furthermore, the LbL polymer coating offers a direct way to functionalize the resonator surface for receptor based chemical sensing applications.

2. EXPERIMENTAL SECTION

2.1. Materials. Poly(4-vinylpyridine) (PVP, M_w = 460 000) and Poly(acrylic acid) (PAA, M_w = 160 000) were purchased from Sigma. (3-Aminopropyl)triethoxysilane (APTES) was purchased from Aladdin Industrial Corporation. All were used as received without further purification. The PAA/PVP solutions were prepared by dissolving PAA or PVP separately into absolute ethanol with different concentrations (0.05−2 mg/mL) and ultrasonicated for 15 min, then incubated overnight at room temperature to get uniform solutions.

2.2. Surface Modification of FBAR. Fabricated FBAR was oxidized first by exposure to air plasma for 5 min to form hydroxyl groups in a plasma cleaner. Followed by vapor phase deposition of APTES under reduced pressure in a desiccator to generate an amino layer on AlN surface.

2.3. LbL Assembly by Dipping and Spinning Methods on FBAR. For dipping method, LbL assembly was accomplished by exposing of NH_2-functionalized FBAR into PAA solution for 2 min and rinsed by absolute ethanol for 30 s. The PAA coated FBAR was then dipped into PVP solution with the same procedure. For multiple layers deposition, a homemade fully automatic dipping robot was used to maintain the uniformity of the polymer layers (see Supporting Information).

dx.doi.org/10.1021/am507640g | ACS Appl. Mater. Interfaces 2015, 7, 950−958

For spinning method, NH_2-functionalized FBAR samples were fixed onto a spin-coating machine. The speed was set at 2000 rpm. PAA/PVP solutions were alternatively pumped onto the surface of FBAR samples with syringes by 200 ul/s for 5 s, then the samples were spin-dried for 15 s. After each deposition step, the samples were rinsed with absolute ethanol for 30 s.

2.4. Surface Characterizations. AlN-Si substrate was prepared by chemical vapor deposition (CVD) of AlN thin film (300 nm) onto silicon substrate as a test sample. FTIR spectrometer (Vertex 70v, Bruker Optics, Germany) was recorded to characterize the amino silanization on AlN film. Contact angle measurement (JC2000DM, Zhongchen) and was used to measure the water contact angle on AlN-Si substrate after amino silanization and LbL assembly. UV−vis spectrometer (TU-1950, Purkinje General Instrument) with a mirror reflection accessory (MR19−1) was employed to record the wavelength shift after every two bilayer depositions. Ellipsometer (EMPro, ElliTop Scientific Co., Ltd.) was used to measure the thickness of PAA/PVP films. The morphology of the deposited thin films on FBAR surface was characterized by atom force microscopy (AFM) (Veeco, Nano Scope III) in tapping mode.

2.5. Reliability Evaluation of FBAR after LbL Assembly through PCT. Five bilayers of PAA/PVP were prepared on FBAR samples by spinning with 0.1 mg/mL PAA/PVP solutions. The samples were then exposed to PCT in a high-pressure chamber where the temperature was set at 110 °C and the humidity at 100% for 12 h.

2.6. NPA Vapor Detection System. Five bilayers of PAA/PVP were spin assembled onto the surface of FBAR with 1 mg/mL of PAA/PVP solutions. After wire-bonding to an evaluation board (EVB), the terminals of EVB were connected to a VNA to real-time record the frequency shift using Matlab. A customized vapor delivery system was introduced to deliver the NPA vapor. In this system, one NPA vapor channel was used to bubble out the NPA vapor by nitrogen gas, while another channel filled with nitrogen gas was only used to adjust the relative concentration of final mixture gas by changing the ratio of two channel flow rate. The total flow rate during the detection was kept constant with the aid of a flow meter monitor. The NPA relative concentration increased after each nitrogen rinse in the detection process.

3. RESULTS AND DISCUSSION

The advantages of FBAR are its high power durability and high resistance to electrostatic discharge (ESD), high quality factor (Q) in the high frequency range and the possibility of realizing monolithic devices with active RF devices.[28] In this work, FBAR is fabricated using standard microfabrication process (see Supporting Information).[27] It comprises three basic layers, a piezoelectric (PZ) layer, a top electrode (TE) and bottom electrode (BE) layer, forming a sandwich structure as illustrated in Figure 1a.[28] An additional passivation (PS) layer on the top of FBAR is to ensure the electrical isolation from ambient and prevent the oxidization of the TE. Aluminum nitride (AlN) is used as both the PZ layer and the PS layer, and molybdenum (Mo) is used as two electrodes. Figure 2 presents the top-view of scanning electron microscope (SEM) image of a FBAR. When adding a layer of mass loading on the top of FBAR, the series resonant frequency, f_s, decreases linearly related to the mass loading in accordance with the classic Sauerbrey equation:[27,29]

$$\frac{\Delta f}{f_s} \approx -\frac{\rho_m d_m}{\rho_0 d_0} \quad (1)$$

where Δf is the frequency shift, ρ_m and ρ_0 are the density of the mass loading layer and the resonator layer, and d_m and d_0 are the thickness of the mass loading layer and the resonator, respectively. (Note that the classic Sauerbrey equation is valid only when the ratio in either side of eq 1 is smaller than 2%.)

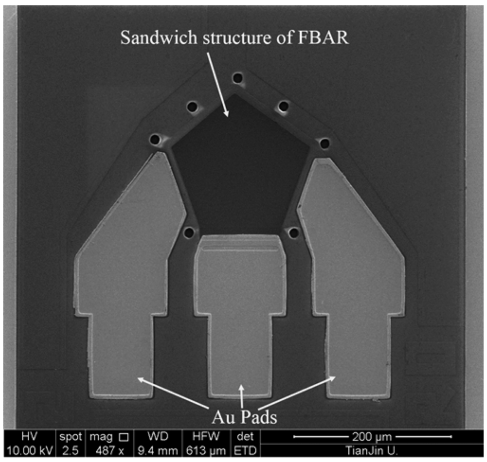

Figure 2. SEM image of a FBAR device (top view after fabrication).

Figure 1 shows the schematic diagram of our tuning process. After silanization of FBAR with APTES, different concentrations of PAA and PVP solutions are deposited onto the FBAR surface (AlN) in a layer by layer fashion. PAA and PVP are selected due to the fact that they are assembled in ethanol which is induced by the hydrogen bonding between the acid and pyridine groups, thus avoids the potential damage of FBAR device if exposed in acid or alkaline solution. Furthermore, it features a linear growth with the increasing number of bilayers, which is favor of precise control of frequency tuning.

3.1. Characterization of LbL Assembly on AlN Film. Unlike silicon or other metal oxides which have been widely applied as substrates for polymer LbL assembly,[30−32] AlN has been rarely reported for its surface modifications.[33−35] In this work, amino silanization and PAA/PVP LbL assembly on AlN were characterized by water contact angle (CA), Fourier transform infrared spectroscopy (FTIR) spectrometer (see Supporting Information), UV−vis reflection spectra, and ellipsometer spectroscopy.

Figure 3 shows the CA results after each step of amino-silanization and PAA/PVP assembly on a flat AlN substrate. After plasma treatment, the water contact angle of AlN drops from 79 to 4° and raises up to 58° after amino-silanization, indicating a successful amino layer coating on AlN. During the LbL assembly, CA values alternate reproducibly between 34−

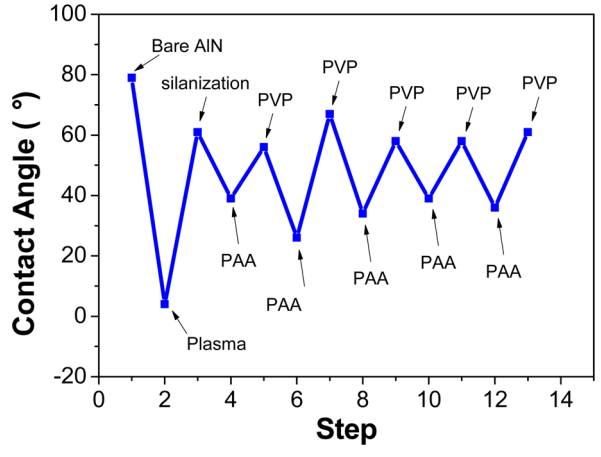

Figure 3. Water contact angle of different layers of PAA/PVP assembly on AlN-Si substrate.

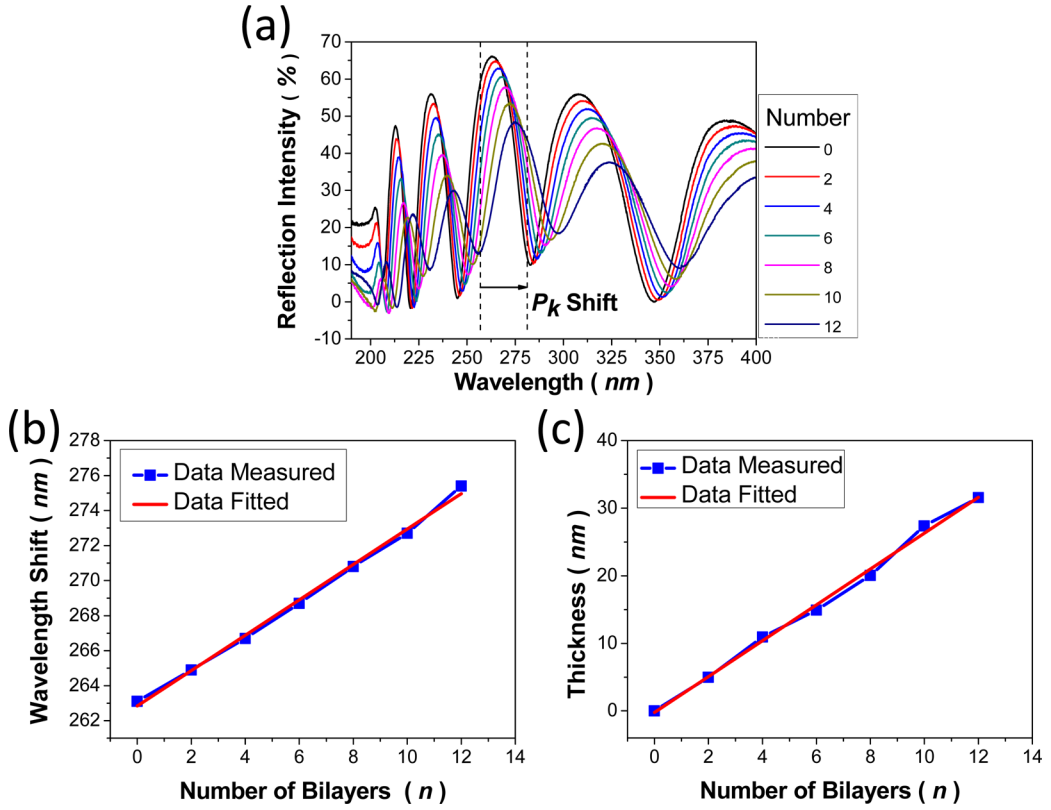

Figure 4. (a) UV−vis reflection spectra measured after each two bilayers of PAA/PVP assembly on AlN surface. (b) Wavelength shift at Pk. (c) Ellipsometer results of the film thickness.

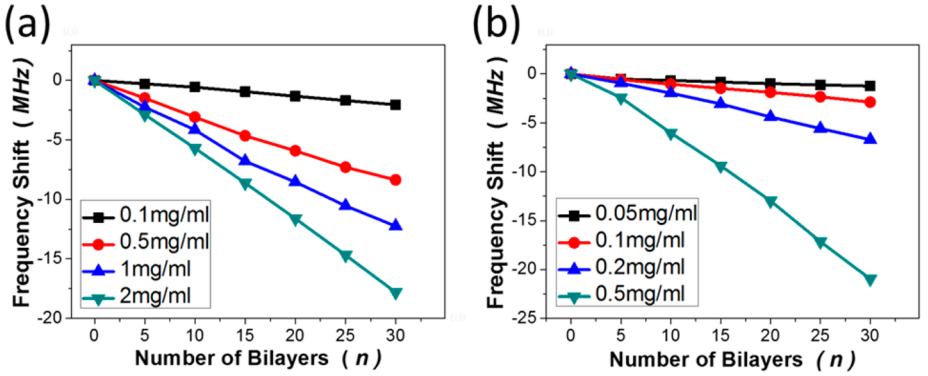

Figure 5. Series resonant frequency shift of FBAR after deposition of every five bilayers with different PAA/PVP concentrations through (a) dipping and (b) spinning-assisted method.

39° (PAA on top) and 58−61° (PVP on top) after the first two bilayers. This proves the successful and successive assembly of PAA/PVP, and the surface property is dominated by the outermost polymer layer. The large deviation of the CA value from the first two bilayers indicates that it takes two complete bilayers to achieve uniform PAA or PVP coatings.[36]

Transmission UV−vis spectrometer is normally applied to monitor the polymer LbL growth on flat substrates, however, it is limited by assembly on UV-transmission substrates (e.g., quartz slides) and presence of UV-absorbing chemical groups from the polymer.[32,37] Because AlN-Si (AlN thin film is grown on silicon as a test substrate) is nontransparent, in this work, we applied UV−vis reflection spectrometer to monitor the PAA/PVP LbL assembly on flat AlN-Si. Instead of intensity signal, the frequency signal (wavelength shift) is recorded to follow the polymer LbL growth. Figure 4a shows the UV−vis reflection spectra measured after each two bilayers of PAA/PVP assembly. The spectra curves are periodically sine-shaped, which is caused by the thin-film interferences with the AlN-Si. The spacing between two successive maximum reflected intensity of one curve becomes larger with the increasing of the wavelength, which can be depicted by free spectral range (FSR) equation.[38] We defined the maximum intensity peak of one curve as characteristic peak (P_k). Figure 4b shows the wavelength shift of P_k during the deposition of PAA/PVP measured by UV−vis reflection spectra. The increase of wavelength at P_k is observed during PAA/PVP deposition which indicates the growth of the polymer layer on AlN-Si. Almost a perfect linear increase of wavelength as a function of the number of bilayers is obtained, and each bilayer corresponds to 1.025 nm wavelength shift, thus indicating the linear growth of PAA/PVP films on AlN substrate.[39] To our

dx.doi.org/10.1021/am507640g | ACS Appl. Mater. Interfaces 2015, 7, 950−958

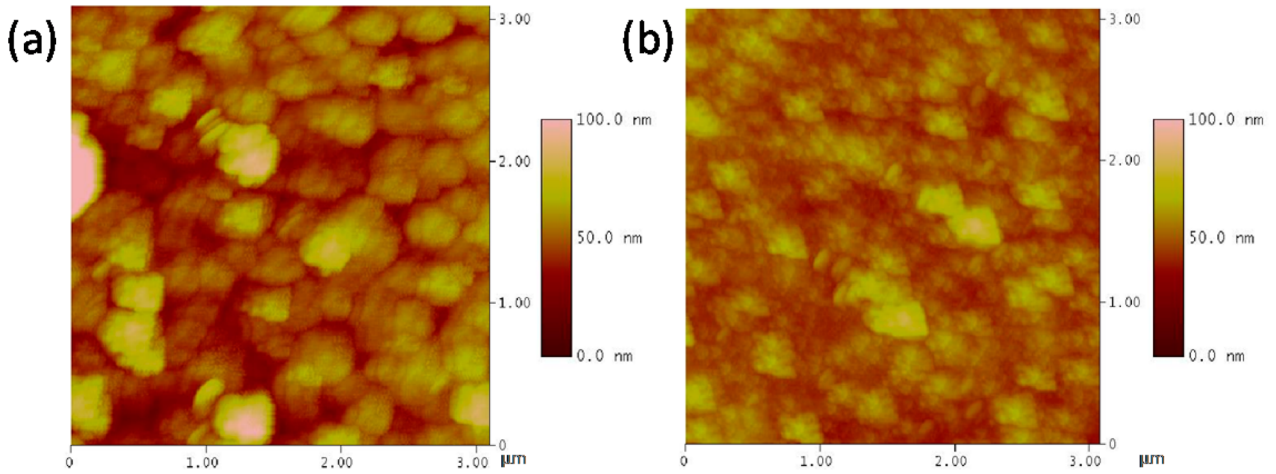

Figure 6. AFM height images show the morphology of PAA/PVP films after 30 bilayers deposition through (a) dipping AlN substrate successively in 2 mg/mL PAA and PVP solutions; the thickness and roughness (RMS) are 86 and 13.4 nm, respectively. (b) Spinning of 0.5 mg/mL PAA and PVP solutions; the thickness and roughness (RMS) are 100.4 and 7.0 nm, respectively.

knowledge, it is the first time UV−vis reflection spectra have been used to characterize polymer LbL growth on non-UV-transparent substrates, and it can be extended to monitor other polymer system even without UV-absorbing chemical groups.

Furthermore, an ellipsometer has been used to monitor the PAA/PVP assembly. Figure 4c shows the film thickness of the PAA/PVP assembly on the same flat AlN-Si substrate after every two bilayer depositions. Again, it confirmed the linear growth of PAA/PVP assembly on AlN and the thickness of each bilayer is measured to be around 2.6 nm. The linear LbL growth of PAA/PVP on AlN-Si is consistent with other reports on quartz or silicon substrates.[39]

3.2. Frequency Tuning by LbL Assembly with Dipping and Spinning Methods. To assist the PAA/PVP LbL assembly on FBAR, dipping and spinning deposition methods are applied in this work.[40] The tuning efficiency, resolution, and morphology of the films are compared.

3.2.1. Dipping Method. PAA/PVP LbL assembly on FBAR was first accomplished by solution dipping method. After amino-silanization, the FBAR devices were exposed alternatively into various concentrations of PAA and PVP solutions, and an ethanol rinsing step was applied between PAA and PVP dipping to remove the physically absorbed polymers. To maintain the uniform coating, we invented a homemade fully automatic dipping robot for multiple polymer layer depositions (>5 layers; see Supporting Information). Figure 5a shows the FBAR frequency shifts measured after every 5 bilayers of PAA/PVP assembly and up to 30 bilayers. Four different concentrations of PAA/PVP are compared to acquire different tuning resolutions. The series resonant frequency is measured through a probe station that connects to an Agilent vector network analyzer (VNA). The result clearly shows a linear decrease of the resonator frequency with the growth of PAA/PVP films, which complies with the UV−vis and ellipsometer results. The series resonant frequency decreases by 8.4 MHz after the deposition of 30 bilayers in 0.5 mg/mL PAA/PVP solutions, meaning each bilayer causes a 0.28 MHz shift. The frequency shift increases with higher concentrations of PAA/PVP, and the minimum frequency tuning of one bilayer is 56 kHZ. By simply controlling the polymer concentration and the number of polymer layers deposited, we can precisely tuning the frequency of FBAR, which is important for real applications of such techniques.

3.2.2. Spinning Method. To further improve the tuning efficiency, we adapted a spinning-assisted LbL assembly using an automatic spinning system to realize high-speed polymer coating (see also Supporting Information). Figure 5b plots the FBAR frequency shift by spinning with different concentrations of polymer solutions. The frequency shift of FBAR with spinning-assisted coating is much larger than that of the dipped coating of the same concentration of PAA/PVP. For example, the series resonant frequency decreased by 20.9 MHz after 30 bilayers deposition in 0.5 mg/mL solutions, meaning each bilayer causes a shift of around 0.6 MHz, which is 2 times higher than that of the dipping method. This phenomenon can be explained by the fast elimination of solvent during the high-speed spinning process, and thus, the concentration of the solutions increases, yielding a higher density of polymer films at FBAR surface.[41] As a result, the maximum series resonant frequency shift of FBAR can reach more than 20 MHz, meaning 1.4% tunability at least. The minimum frequency shift is nearly 10 kHZ per bilayer, indicating a 7 ppm tuning resolution. We also noticed from AFM height images (Figure 6) that the morphology of PAA/PVP film fabricated by the spinning method is smoother. This is caused by the air shear force at the interface between the films and the atmosphere when the coating is deposited at high spinning speed; this shear force planarizes the surface of PAA/PVP films.[41]

3.2.3. Selective Deposition of PAA/PVP Films on AlN Surface over Gold Pads. Selective deposition of polymers on AlN surface over gold pads is very important for device real application, which enables the subsequent packaging and wire-bonding to peripheral circuit. The conventional method requires multiple steps of lithography to achieve selective deposition, which is complicated and cannot be applied to a single diced device. In this work, the amino silanization is only reacted on the AlN surface (there are no hydroxyl groups generating on gold during oxygen plasma), resulting in selective deposition of PAA/PVP on AlN without contaminating the gold pads. This approach has the advantages of mask-less fabrication, and it can be applied to individual diced device. Practically, we observed slight organic contaminations on gold pads during the PAA/PVP LbL assembly which is likely due to

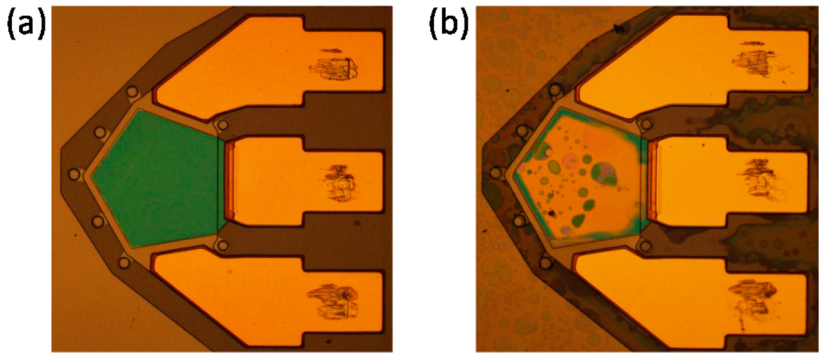

Figure 7. Optical microscope images of FBAR samples after PCT for 12 h. (a) FBAR sample with 5 PAA/PVP bilayers coating. (b) Bare FBAR sample.

the negatively charged gold surface to induce the nonspecific physical absorption of PVP. In this situation, hot solvent is applied in the rinsing step. For instance, ethanol is heated up to 60 °C and stirred with a magnet bar during rinsing step after PAA/PVP deposition. Thirty cycles of deposition of PAA/PVP on gold substrates followed by hot ethanol rinsing was performed and there was no PAA/PVP film observed on gold as confirmed by the ellipsometer. Stirring and heating during the rinsing step ensure the selective deposition of PAA/PVP assembly on AlN.

3.3. Reliability Enhancement of FBAR after LbL Assembly. It is known that the humid atmosphere has a strong negative effect on the reliability of electronic devices. Here, we conducted a pressure cooker test (PCT) to evaluate the moisture resistance of PAA/PVP coatings in extreme environment (at 110 °C and 100% humidity). Figure 7 compares the optical microscope images of FBAR samples with and without PAA/PVP LbL coatings. After PCT for 12 h, there is no obvious damage on PAA/PVP-coated FBAR, while the bare FBAR shows clear damages (Figure 7b).

The Q value is an important parameter of the resonators which indicates the power losses and resonator performance in the system. The device reliability can be monitored by the Q value of FBAR calculated from eq 2:[28]

$$Q = \frac{2*\pi*f*\tau*|S_{11}|}{1 - |S_{11}|^2} \quad (2)$$

where S_{11} is the scatter parameter, f represents the FBAR resonant frequency, and τ is the group delay of the S_{11}.

Table 1 shows the Q value of FBAR as a function of time during the PCT process, there is no Q value dropping from the devices coated with PAA/PVP (samples 1 and 2), whereas the Q value of bare FBAR (samples 3 and 4) decreases largely which is likely caused by the water vapor corrosion of the AlN layer and the interface of different material layers. The results are complied with the optical results. PAA/PVP LbL coating serves as a second passivation layer that prevents the contact of FBAR with water vapor. This proves that LbL assembly not only tunes the resonant frequency but also serves as a protection layer to enhance the device reliability for practical applications.

Table 1. Q Value of Four FBARs as a Function of Time in the PCT Process[a]

period	sample 1	sample 2	sample 3	sample 4
0 h	1372	1517	1208	1440
12 h	1530	1675	283	673

[a]Samples 1 and 2 are coated with PAA/PVP, while samples 3 and 4 are not.

3.4. Applications of PAA/PVP LbL Coated FBAR. *3.4.1. Tuning Band Pass Filter in Wireless Broadband Communication.* As one application of LbL coated FBAR, two-port FBAR filters used in wireless broadband communication are fabricated to verify the frequency tuning performance after polymer LbL assembly. FBAR has been widely applied in the field of RF filters, which are formed with the ladder or lattice topologies by series and parallel connection of several FBARs, even the topologies can be cascaded to give better selectivity.[42] The resonant frequency of FBARs were used to determine the pass band of the filter. When the pass band deviates from a given one in the wireless broadband communication, the calling quality will degrade. It is crucial to tune the pass band to a specific band exactly. The tuning result of the FBAR filters after 10 bilayers of PAA/PVP assembly (0.1 mg/mL) is shown in Figure 8. Figure 8a,b shows optical images of the FBAR filters before and after PAA/PVP assembly; no defect was observed after LbL deposition. Figure 8c,d compares the electric performance in both wide and narrow band before (red line) and after (blue line) the PAA/PVP assembly. After 10 bilayers deposition, the pass band shifts down by 8 MHz at −20 dB while the performance in pass band and stop band maintain the same. The insertion loss does not fail anymore which demonstrates the feasibility of the real application of this technique.

3.4.2. Signal Enhancement in Gas Sensing. One major application of microfabricated resonators is in chemical sensors in which chemical receptors are immobilized on the sensor surface to interact and induce analyte adsorption, thus producing mass loading on top of the resonators, which can be detected as a shift of the resonant frequency.[2,29] Besides the frequency tuning, the polymer LbL assembly offers a direct way to chemically functionalize the resonators and facilitates their chemical sensing.

Here, we demonstrated the frequency tuning and further sensing of n-propyl alcohol (NPA) vapors with PAA/PVP LbL coated FBAR. Two FBAR samples with different original f_s were used. Sample 1 was coated with amino silane (APTES) as a monolayer, which does not change its original f_s. Sample 2 was coated with five bilayers of PAA/PVP through spin-assisted LbL assembly, which reduces the original f_s from 1442.3 to 1435.0 MHz. After coating, the f_s variation of these two FBARs was narrowed down to 0.3 MHz from 7 MHz, which facilitates

dx.doi.org/10.1021/am507640g | ACS Appl. Mater. Interfaces 2015, 7, 950−958

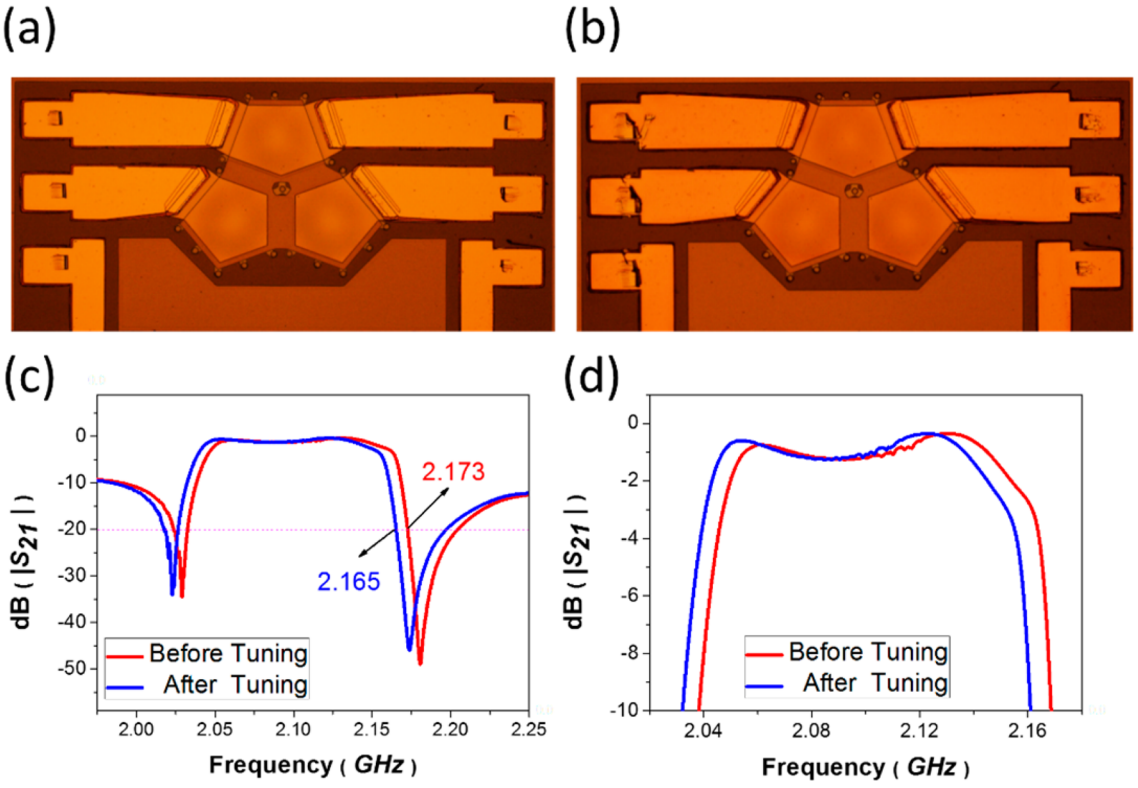

Figure 8. Tuning of FBAR filters using molecular LbL self-assembly approach for wireless broadband communication. Optical microscope images of a FBAR filter (a) before and (b) after LbL assembly. Electrical performance of (c) wide band and (d) pass band (red) before and (blue) after LbL assembly.

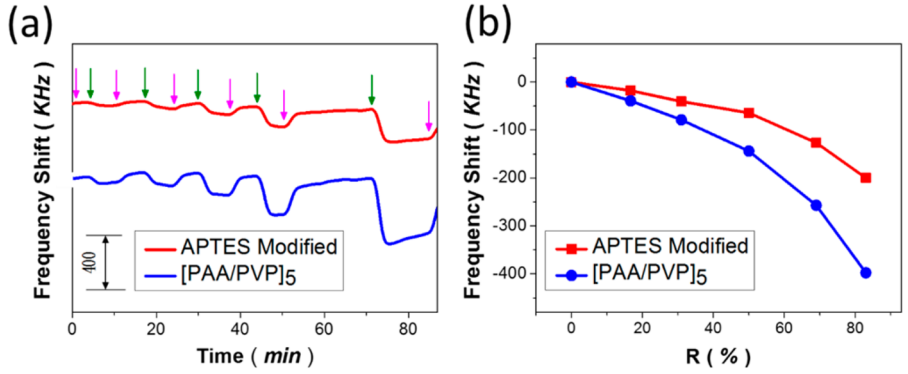

Figure 9. Responses of APTES- and $[PAA/PVP]_5$-modified FBAR for NPA sensing. (a) Time course of frequency shift when the two FBAR samples are exposed to a set of different NPA relative concentrations; (pink arrows) nitrogen flow and (green arrows) injection of NPA. (b) The extracted frequency shift as a function of NPA relative concentration.

the further comparison of their gas sensing result. Figure 9a shows the real time sensor responses of the two FBARs exposed to a continuous NPA vapors with a set of different NPA relative concentrations. We define the relative concentration (R) of the NPA vapors as the ratio of NPA vapor flow rate to the total gas flow rate (NPA and nitrogen):

$$R = \frac{FR_{\mathrm{NPA}}}{FR_{\mathrm{NPA}} + FR_{\mathrm{Nitrogen}}} \quad (3)$$

Where FR_{NPA} and FR_{Nitrogen} are the flow rate of NPA vapor and nitrogen gas, respectively.

It clearly shows that the resonant frequency decreases when exposed to NPA vapors and frequency shift increases with higher NPA concentrations for both samples 1 and 2, which indicates the chemical adsorption of NPA on FBAR surface. However, the sensor response is much higher for $[PAA/PVP]_5$-coated FBAR compared with that of APTES-coated FBAR, as indicated in Figure 9b. The signal enhancement with PAA/PVP LbL coating is likely due to its loose structure from the multilayer coating which can absorb more NPA vapors.[43] It proves that the LbL polymer coating of the resonant sensors functions both as frequency tuning and sensor surface functionalization for chemical sensing applications.

4. CONCLUSIONS

In this work, we introduced a new method to tune the resonant frequency of microfabricated resonators using molecular LbL self-assembly approach. PAA/PVP coating on FBAR surface has

dx.doi.org/10.1021/am507640g | ACS Appl. Mater. Interfaces 2015, 7, 950−958

been used as an example to demonstrate the procedure. The film thickness and morphology have been characterized by different techniques for both dipping and spinning-assisted assembly. The tunability, resolution, and device reliability are also evaluated. The frequency tuning using molecular LbL coating shows great advantages: it is a maskless process, and the polymer can be directly and selectively assembled on the resonator surface through molecular recognition, which avoids the high-cost conventional semiconductor fabrications and is able to tune the individual diced device.

The molecular LbL surface coated FBARs are demonstrated in real applications to tune the FBAR filters and to detect NPA vapors as enhanced chemical sensors. It is worth mentioning that the coated polymer films can be completely removed by simple oxygen plasma treatment (see Supporting Information), thus allowing the regeneration of the resonators, which are attractive from both the resonator performance and economical point of view. Furthermore, such a frequency tuning method can be applied to other resonators for varies applications as well.

■ ASSOCIATED CONTENT

Supporting Information

FBAR fabrication process, distribution of working frequency diagram of FBAR filters from a 4 in. wafer level after fabrication, contact angle images, homemade fully automatic dipping robot and spinning system, UV−vis reflection spectra. This material is available free of charge via the Internet at http://pubs.acs.org.

■ AUTHOR INFORMATION

Corresponding Authors

*E-mail: xduan@tju.edu.cn.
*E-mail: haozhang@tju.edu.cn.

Notes

The authors declare no competing financial interest.

■ ACKNOWLEDGMENTS

The authors gratefully acknowledge financial support in part from the Natural Science Foundation of China (NSFC No. 61176106) and the 111 Project (B07014). X.D. acknowledges support by the Tianjin Applied Basic Research and Advanced Technology (14JCYBJC41500). We are grateful to our colleague Dr. Bin Yuan for help on the polymer deposition and helpful discussions.

■ REFERENCES

(1) Li, W.; Liu, Z.; Lin, H.; Nie, Z.; Chen, J.; Xu, X.; Yao, S. Label-Free Colorimetric Assay for Methyltransferase Activity Based on a Novel Methylation-Responsive Dnazyme Strategy. *Anal. Chem.* **2010**, *82*, 1935−1941.

(2) Chiu, C. S.; Gwo, S. Quantitative Surface Acoustic Wave Detection Based on Colloidal Gold Nanoparticles and Their Bioconjugates. *Anal. Chem.* **2008**, *80*, 3318−3326.

(3) Auer, S.; Nirschl, M.; Schreiter, M.; Vikholm-Lundin, I. Detection of DNA Hybridisation in a Diluted Serum Matrix by Surface Plasmon Resonance and Film Bulk Acoustic Resonators. *Anal. Bioanal. Chem.* **2011**, *400*, 1387−1396.

(4) Campanella, H.; Uranga, A.; Romano-Rodriguez, A.; Montserrat, J.; Abadal, G.; Barniol, N.; Esteve, J. Localized-Mass Detection Based on Thin-Film Bulk Acoustic Wave Resonators (FBAR): Area and Mass Location Aspects. *Sens. Actuators, A* **2008**, *142*, 322−328.

(5) Zhao, X.; Pan, F.; Ashley, G. M.; Garcia-Gancedo, L.; Luo, J.; Flewitt, A. J.; Lu, J. R. Label-Free Detection of Human Prostate-Specific Antigen (hPSA) Using Film Bulk Acoustic Resonators (FBARs). *Sens. Actuators, B* **2014**, *190*, 946−953.

(6) Länge, K.; Rapp, B. E.; Rapp, M. Surface Acoustic Wave Biosensors: A Review. *Anal. Bioanal. Chem.* **2008**, *391*, 1509−1519.

(7) Kadota, M.; Nakao, T.; Taniguchi, N.; Takata, E.; Mimura, M.; Nishiyama, K.; Komura, T. Surface Acoustic Wave Duplexer for US Personal Communication Services With Good Temperature Characteristics. *Jpn. J. Appl. Phys., Part 1* **2005**, *44*, 4527.

(8) Hara, M.; Yokoyama, T.; Sakashita, T.; Taniguchi, S.; Iwaki, M.; Nishihara, T.; Satoh, Y. Super-High-Frequency Band Filters Configured with Air-Gap-Type Thin-Film Bulk Acoustic Resonators. *Jpn. J. Appl. Phys.* **2010**, *49*, 07HD13.

(9) Khine, L.; Wong, L. Y.; Soon, J. B.; Tsai, M. L. J. FBAR Resonators with Sufficient High Q for RF Filter Implementation. *Adv. Mater. Res.* **2011**, *254*, 70−73.

(10) Sazonova, V.; Yaish, Y.; Üstünel, H.; Roundy, D.; Arias, T. A.; McEuen, P. L. A Tunable Carbon Nanotube Electromechanical Oscillator. *Nature* **2004**, *431*, 284−287.

(11) Zuo, G.; Li, X.; Zhang, Z.; Yang, T.; Wang, Y.; Cheng, Z.; Feng, S. Dual-SAM Functionalization on Integrated Cantilevers for Specific Trace-Explosive Sensing and Non-Specific Adsorption Suppression. *Nanotechnology* **2007**, *18*, 255501.

(12) Park, J. Y.; Lee, K. H.; Cheon, S. J. Silicon Bulk Micromachined FBAR Filter and Duplexer for Advanced Handset Applications. *Microwave Opt. Technol. Lett.* **2007**, *49* (2), 339−342.

(13) Nagai, Y.; Carbajal, J. D.; White, J. H.; Sladek, R.; Grutter, P.; Lennox, R. B. An Electrochemically Controlled Microcantilever Biosensor. *Langmuir* **2013**, *29*, 9951−9957.

(14) Tigli, O.; Zaghloul, M. E. A Novel SAW Device in CMOS: Design, Modeling, and Fabrication. *Sensors J. IEEE* **2007**, *7*, 219−227.

(15) Lassagne, B.; Garcia-Sanchez, D.; Aguasca, A.; Bachtold, A. Ultrasensitive Mass Sensing with a Nanotube Electromechanical Resonator. *Nano Lett.* **2008**, *8*, 3735−3738.

(16) Chiu, H. Y.; Hung, P.; Postma, H. W. C.; Bockrath, M. Atomic-Scale Mass Sensing Using Carbon Nanotube Resonators. *Nano Lett.* **2008**, *8*, 4342−4346.

(17) Feng, X. L.; He, R.; Yang, P.; Roukes, M. L. Very High Frequency Silicon Nanowire Electromechanical Resonators. *Nano Lett.* **2007**, *7*, 1953−1959.

(18) Zande, A. M. V. D.; Barton, R. A.; Alden, J. S.; Ruiz-Vargas, C. S.; Whitney, W. S.; Pham, P. H.; McEuen, P. L. Large-Scale Arrays of Single-Layer Graphene Resonators. *Nano Lett.* **2010**, *10*, 4869−4873.

(19) Castellanos-Gomez, A.; van Leeuwen, R.; Buscema, M.; van der Zant, H. S.; Steele, G. A.; Venstra, W. J. Single-Layer MoS_2 Mechanical Resonators. *Adv. Mater.* **2013**, *25*, 6719−6723.

(20) Arlett, J. L.; Myers, E. B.; Roukes, M. L. Comparative Advantages of Mechanical Biosensors. *Nat. Nanotechnol.* **2011**, *6*, 203−215.

(21) Verbridge, S. S.; Shapiro, D. F.; Craighead, H. G.; Parpia, J. M. Macroscopic Tuning of Nanomechanics: Substrate Bending for Reversible Control of Frequency and Quality Factor of Nanostring Resonators. *Nano Lett.* **2007**, *7*, 1728−1735.

(22) Huttel, A. K.; Steele, G. A.; Witkamp, B.; Poot, M.; Kouwenhoven, L. P.; van der Zant, H. S. Carbon Nanotubes as Ultrahigh Quality Factor Mechanical Resonators. *Nano Lett.* **2009**, *9*, 2547−2552.

(23) Sukhorukov, G. B.; Antipov, A. A.; Voigt, A.; Donath, E.; Möhwald, H. pH-Controlled Macromolecule Encapsulation in and Release from Polyelectrolyte Multilayer Nanocapsules. Macromol. *Rapid Commun.* **2001**, *22*, 44−46.

(24) Caruso, F.; Rodda, E.; Furlong, D. N.; Niikura, K.; Okahata, Y. Quartz Crystal Microbalance Study of DNA Immobilization and Hybridization for Nucleic Acid Sensor Development. *Anal. Chem.* **1997**, *69*, 2043−2049.

(25) Biggs, S.; Sakai, K.; Addison, T.; Schmid, A.; Armes, S. P.; Vamvakaki, M.; Webber, G. Layer-by-Layer Formation of Smart Particle Coatings Using Oppositely Charged Block Copolymer Micelles. *Adv. Mater.* **2007**, *19*, 247−250 (2007).

(26) Kharlampieva, E.; Kozlovskaya, V.; Sukhishvili, S. A. Layer-by-Layer Hydrogen-Bonded Polymer Films: From Fundamentals to Applications. *Adv. Mater.* **2009**, *21*, 3053−3065.
(27) Zhang, H.; Marma, M. S.; Kim, E. S.; McKenna, C. E.; Thompson, M. E. A Film Bulk Acoustic Resonator in Liquid Environments. *J. Micromech. Microeng.* **2005**, *15*, 1911.
(28) Hashimoto, K. Y., Ed. *RF Bulk Acoustic Wave Filters for Communications*. Artech House: London, 2009.
(29) Pang, W.; Zhao, H.; Kim, E. S.; Zhang, H.; Yu, H.; Hu, X. Piezoelectric Microelectromechanical Resonant Sensors for Chemical and Biological Detection. *Lab Chip* **2012**, *12*, 29−44.
(30) Shi, F.; Liu, Z.; Wu, G. L.; Zhang, M.; Chen, H.; Wang, Z. Q.; Willner, I. Surface Imprinting in Layer-by-Layer Nanostructured Films. *Adv. Funct. Mater.* **2007**, *17*, 1821−1827.
(31) Mayya, K. S.; Schoeler, B.; Caruso, F. Preparation and Organization of Nanoscale Polyelectrolyte-Coated Gold Nanoparticles. *Adv. Funct. Mater.* **2003**, *13*, 183−188.
(32) Xu, H.; Gomez-Casado, A.; Liu, Z.; Reinhoudt, D. N.; Lammertink, R. G.; Huskens, J. Porous Multilayer-Coated PDMS Stamps for Protein Printing. *Langmuir* **2009**, *25*, 13972−13977.
(33) Baur, B.; Steinhoff, G.; Hernando, J.; Purrucker, O.; Tanaka, M.; Nickel, B.; Eickhoff, M. Chemical Functionalization of Gan and AlN Surfaces. *Appl. Phys. Lett.* **2005**, *87*, 263901.
(34) Chiu, C. S.; Lee, H. M.; Kuo, C. T.; Gwo, S. Immobilization of DNA-Au Nanoparticles on Aminosilane-Functionalized Aluminum Nitride Epitaxial Films for Surface Acoustic Wave Sensing. *Appl. Phys. Lett.* **2008**, *93*, 163106.
(35) Chen, C. F.; Wu, C. L.; Gwo, S. Organosilane Functionalization of Inn Surface. *Appl. Phys. Lett.* **2006**, *89*, 252109.
(36) Yoo, D.; Shiratori, S. S.; Rubner, M. F. Controlling Bilayer Composition and Surface Wettability of Sequentially Adsorbed Multilayers of Weak Polyelectrolytes. *Macromolecules* **1998**, *31*, 4309−4318.
(37) Moon, J. H.; Shin, J. W.; Kim, S. Y.; Park, J. W. Formation of Uniform Aminosilane Thin Layers: An Imine Formation to Measure Relative Surface Density of the Amine Group. *Langmuir* **1996**, *12*, 4621−4624.
(38) Nawrocka, M. S.; Liu, T.; Wang, X.; Panepucci, R. R. Tunable Silicon Microring Resonator with Wide Free Spectral Range. *Appl. Phys. Lett.* **2006**, *89*, 071110.
(39) Fu, Y.; Bai, S.; Cui, S.; Qiu, D.; Wang, Z.; Zhang, X. Hydrogen-Bonding-Directed Layer-by-Layer Multilayer Assembly: Reconformation Yielding Microporous Films. *Macromolecules* **2002**, *35*, 9451−9458.
(40) Seo, J.; Lutkenhaus, J. L.; Kim, J.; Hammond, P. T.; Char, K. Effect of the Layer-by-Layer (LbL) Deposition Method on the Surface Morphology and Wetting Behavior of Hydrophobically Modified PEO and PAA LbL Films. *Langmuir* **2008**, *24*, 7995−8000.
(41) Cho, J.; Char, K.; Hong, J. D.; Lee, K. B. Fabrication of Highly Ordered Multilayer Films Using a Spin Self-Assembly Method. *Adv. Mater.* **2001**, *13*, 1076−1078.
(42) Wang, K.; Frank, M.; Bradley, P.; Ruby, R.; Mueller, W.; Barfknecht, A.; Gat, M. FBAR Rx Filters for Handset Front-End Modules with Wafer-Level Packaging. *2003 IEEE Symposium on Ultrasonics* **2003**, *1*, 162−165.
(43) Korposh, S.; Selyanchyn, R.; Lee, S. W. Nano-assembled Thin Film Gas Sensors. IV. Mass-Sensitive Monitoring of Humidity Using Quartz Crystal Microbalance (QCM) Electrodes. *Sens. Actuators, B* **2010**, *147*, 599−606.